Chapter

Middle Miocene Evaporites from Northern Iraq: Petrography, Geochemistry, and Cap Rock Efficiency

Ali I. Al-Juboury, Rana A. Mahmood and Abulaziz M. Al-Hamdani

Abstract

Evaporites (gypsum and anhydrite) of the middle Miocene age (Fat'ha Formation) form one of the main sulfate cap rocks in the Middle East oilfields. Detailed petrographic and diagenetic investigations accompanied with geochemical analysis of these evaporite rocks in Mosul and Kirkuk areas of northern Iraq have revealed that nodular gypsum is the dominant type, whereas laminated, structureless, and secondary (selenite and satin spar) also are present. Nodular gypsum was deposited in a very shallow, arid, and semi-restricted lagoonal environment which has undergone influx and reflux processes, while laminated gypsum may represent pulses of freshwater into the lagoonal basin of Fat'ha Formation. Low strontium values of the secondary and laminated gypsum may attribute to their secondary origin by hydration processes from the original anhydrite. Based on petrographic, diagenetic, and petrophysical (porosity and permeability) properties, it appears that the efficiency of the Fat'ha sulfates as petroleum cap rocks increases with increasing nodular growth and compaction degree. The occasional presence of bitumen inclusions with both nodular gypsum and host materials relates to early leakage of the hydrocarbons which were being halt due to the growing and packing of nodules and host materials.

Keywords: evaporites, petrography, geochemistry, cap rock potential, miocene, Iraq

1. Introduction

More than 70% of the world's giant oilfields in carbonate rocks bear a relationship to evaporites [1]. The association among evaporates, carbonates, and hydrocarbons is more than fortuitous as evaporates constitute less than 2% of the world's platform sediments [2].

Evaporites form about 50% of the total thickness of the middle Miocene Fat'ha Formation in Iraq [3]. Gypsum ($CaSO_4.2H_2O$) is the most common type in surface (outcrop) sections, while in subsurface sections, anhydrite ($CaSO_4$) and halite (NaCl) are the most common evaporites.

The Fat'ha Formation was deposited in a NW-SE-oriented basin which extended from NE Syria through N and NE Iraq into SW Iran (**Figure 1**). This basin is called the "Mesopotamian Basin" which is a foreland basin situated on the leading edge of the Arabian Plate attached to the African Plate [3].

The basin-center model is also manifested by the concentric arrangement of evaporite beds interbedded with limestone and marly limestone with gypsum and anhydrite along the margins to soluble halite in the depocenter. During high-frequency sea-level lowstands, intra-basinal and regional structural barriers may have isolated the hypersaline basin from the open sea, such that evaporation exceeded

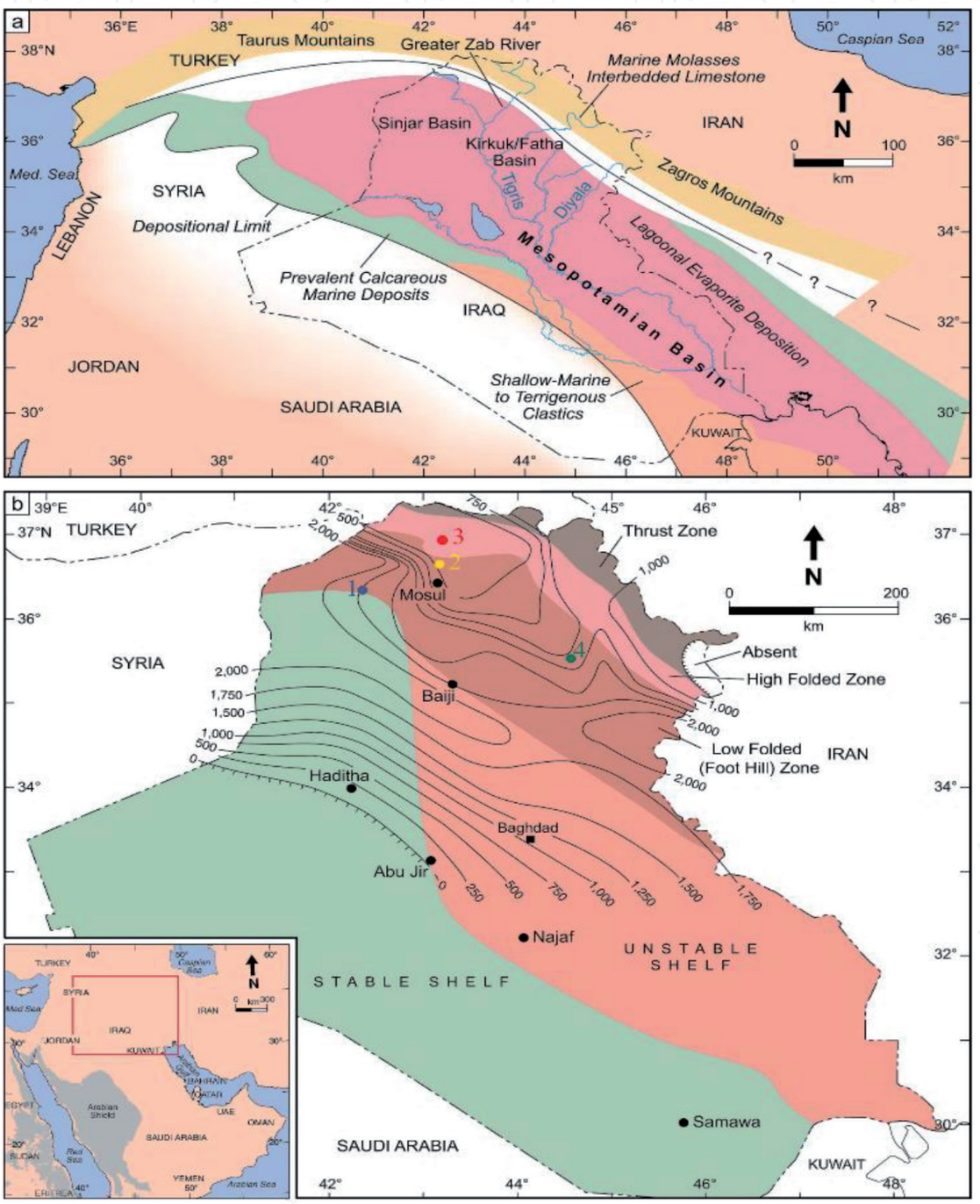

Figure 1.
(a) Location map showing the Mesopotamian Basin in Iraq and Fat'ha/Kirkuk and Sinjar sub-basins. Simplified middle Miocene lithofacies distribution map (after [4–7]). (b) Locations of the four studied sections: (1) Sheikh Ibrahim, (2) Telkif, (3) Batnaya, and (4) well in Kirkuk. Also shown is an isopach map of the Fat'ha Formation (after [4]) and tectonic provinces of Iraq (modified from [3] after permission from GeoArabia).

the ingress of water in an arid climate [2, 3]. The Fat'ha Formation is one of the most extensive and economically important formations in the entire Middle East region [8].

The formation covers a large area (approximately 1500 km x 300 km) and extends northwestward into Syria (there termed Lower Fars Formation) and southeastward into Iran (there termed upper part Gachsaran Formation) [9] (**Figure 1**). The Fat'ha Formation is a seal to numerous oil reservoirs in Iraq and Iran and, in certain areas, is a reservoir in its own right (e.g., Kirkuk, northern Iraq, [4, 10]).

In the present study, lithofacies analyses of various gypsum and anhydrite successions from both surface and subsurface sections (**Figure 1**) are studied accompanied by petrographic investigation using traditional petrographic microscope supported by scanning electron microscopy (SEM) for better determination of their petrographic, textural, and diagenetic features. The study also includes mineralogical determination using X-ray diffraction (XRD), geochemical, X-ray fluorescence (XRF), and petrophysical (porosity and permeability) measurements for selected samples from both surface and subsurface sections.

The aim of the study is to elucidate the lithofacies and related petrographic, textural, and diagenetic and geochemical characteristics of the gypsum and anhydrites of the Fat'ha Formation and to determine their ability as seal or cap rocks.

2. Geologic setting

The Neo-Tethys Ocean began to close in the late Cretaceous as evidenced by the obduction of ophiolites in Oman and elsewhere along the margin of the Arabian Plate [11, 12]. In the late Miocene and early Pliocene, the Neo-Tethys Ocean was closed by the collision of the Arabian and Eurasian plates (Central Iran and Turkey), and the Zagros and Taurus Mountain belts started to be uplifted [13, 14]. Between these two tectonic events, starting in the late Eocene and continuing through the middle Miocene, crustal loading and flexure of the eastern Arabian Plate formed the broad and shallow Mesopotamian Basin as a NW-oriented foreland basin [15, 16]. This 2000-km-long basin extended from Bandar Abbas, in Iran, across Iraq and Syria to the Mediterranean Sea, and it was located southwest of the Zagros and Taurus Mountains (**Figure 1**).

The Fat'ha Formation is largely an evaporatic sequence. It consists of numerous shallowing-upward cycles of alternating mudrocks, limestones, gypsum, anhydrite, and halite which are present in the basin center. The rich sulfur deposits are found in evaporite beds consisting mainly of gypsum and anhydrite, limestone, marl, and claystone [17]. The formation comprises a cyclic succession deposited in shallow marine, supra-tidal, and continental environments [5, 18]. The formation of the Zagros-Taurus mountain range led to the development of the Mesopotamian Basin as a result of crustal loading and flexure. Major orogeny also occurred in the late Miocene–Pliocene as a result of regional changes in the rates of plate motion, which produced a preferential northward movement of the Arabian Plate relative to the Iranian-Turkish plates, and the collision of the Turkish-Iranian plates with the Eurasian plate to the north.

3. Materials and methodology

Forty five samples from the middle Miocene evaporate succession were selected for the present work. Lithofacies analysis is conducted in the field based on

systematic classification of gypsum/anhydrite by Holliday (1971) [19] and comparison with classifications of [20, 21].

Petrographic investigation using traditional petrographic microscopy are achieved at the Geology Department of Mosul University, Iraq. Furthermore, a deeply focusing of textural and diagenetic identification using scanning electron microscopy (SEM) was conducted on selected samples using Camscan MV 2300 SEM at Steinmann Institute, Bonn University, Germany. Mineralogical XRD analysis using D8 ADVANCE [Bruker AXS] with Cu-∞radiation and geochemical analysis using Siemens SRS 303 XRF also are conducted at Steinmann Institute, Bonn University, Germany, whereas porosity and permeability measurements were conducted at the Geology Department of University of Mosul, Iraq, using dimension measurement and wax method using Soxlith instrument after bitumen extraction for porosity and the pipette method for permeability measurement, respectively.

4. Results

4.1 Lithofacies

Several lithofacies have been recognized through the field study of the evaporitic successions of the Fat'ha Formation; these include the following:

1. Nodular and structureless gypsum/anhydrite lithofacies

This form is the common lithofacies in the studied successions. They are commonly bedded with thickness varying between 0.1 and 50 meters. Nodules are white sucrose or of other colors depending on the included impurities. These nodules are surrounded by different colors of clayey or carbonate stripes. Nodules are finger-shaped or cylindrical in the lower parts of the beds to condensed circle in shape in the upper parts (**Figure 2A**) or as compound nodular texture (**Figure 2B**).

Based on the nature of the nodules and their interstitial materials, compaction and growth nature of these nodules, deformation features, and nature of bedding, several sublithofacies could be recognized, and these include nodular, nodular mosaic, mosaic, wispy, and massive (structureless) gypsum/anhydrite sublithofacies (see **Figures 2**–**4**). Laminated and enterolithic structures (as a result of anhydrite to gypsum transformation) are common in the mosaic secondary sublithofacies. This lithofacies could be correlated with the Miocene sulfate facies of Seven River Formation of southeast Mexico [22], Codo Formation evaporate of northern Brazil [23], and middle Miocene gypsum unit (Ninyerola) near Valencia, Italy [24].

2. Laminated gypsum lithofacies

This lithofacies is less dominated than the previous one and characterized by thin lamination with lamina of less than 2 mm thick and interlaminated with other marly, limy, or secondary satin spar or selenite laminas (see **Figures 2F** and **3F**). This interlamination may reflect cyclic dynamic changes of the sedimentary basin where the thickness of lamina reflects the stability period of the basin [25]. The gypsum laminas are formed of fine white sucrose (alabastrine type) of gypsum, whereas other laminas are of pale to greenish-gray in color. This color variation may reflect the seasonal changes in temperature and water chemistry of the basin [25].

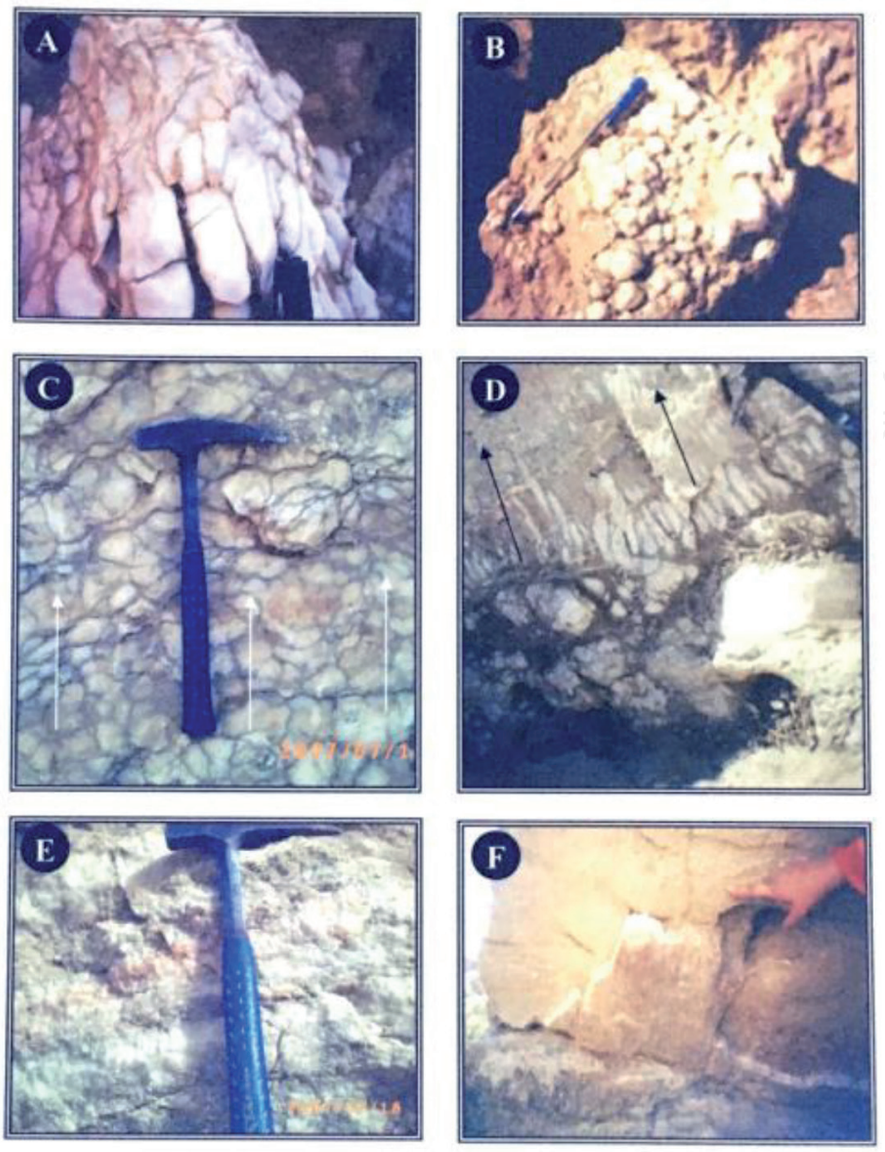

Figure 2.
(A) Elongated nodules in the lower part of the gypsum beds. (B) Compound spherical gypsum nodules as representative for the compound nodular lithofacies. (C) Gradual change of mosaic to wispy gypsum upward. (D) Gradual change of singular to compound nodular to mosaic then to wispy and massive structureless gypsum. (E) Gypsum bed composed of alternative mosaic nodules. (F) Satin spar laminas fill bedding planes in gypsum bed, Sheikh Ibrahim section.

3. Satin spar and selenite gypsum lithofacies

This lithofacies is dominated in the evaporate successions of the Fat'ha Formation and in their interlaminated marly, clayey, and limestone beds as veins, lenses, and fibrous nodules along bedding planes or within joints, cracks, and cavities and commonly is dominated in the upper parts of the formation. Two sublithofacies are recognized in the present study, satin spar and selenite (**Figure 5**).

4.2 Petrography and diagenesis

4.2.1 Petrographic investigation

Detailed petrographic analysis of the studied evaporitic succession by the means of polarized microscopy supported by scanning electron microscopic study has revealed that nodular gypsum is the dominant gypsum type, although laminated

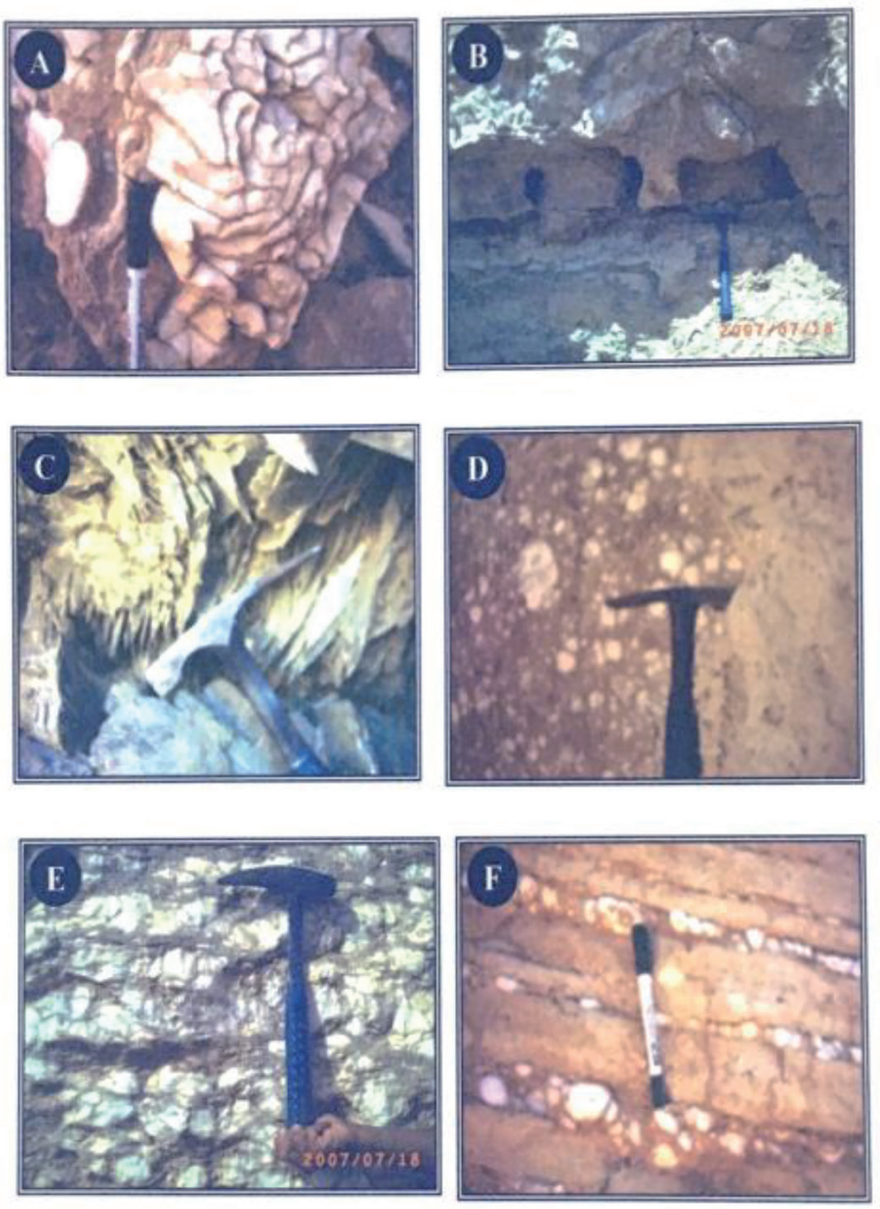

Figure 3.
(A) Enterolithic structure. (B) Erosional caving in the lower part of the gypsum bed within marl hosting nodular gypsum. (C) Desert rose feature in secondary gypsum forming large twinned laminas of fibrous gypsum. (D) Lime interstitial materials in between spherical gypsum nodules. (E) Sutured marly materials in between gypsum nodules in thinly laminated gypsum unit. (F) Laminated nodular gypsum beds with marl (A, C, D, F—Sheikh Ibrahim section; B—Batnaya; and E—Telkif section).

and thick-bedded gypsum are also present. Nodular gypsum passes gradually and vertically into thick to very thick-bedded gypsum. Secondary gypsum (selenite and satin spar) also occurs. Gypsum is white and sugary or creamy in color, but red pink and greenish white varieties also are present. The greenish white color is usually related to secondary coloration as result of enveloping cover of green marl in the succession of the Fat'ha Formation.

In the current study, several textures for gypsum and anhydrite are recognized.

Gypsum textures: Four principal textures are distinguished, some are subdivided into secondary types based on the form, size, and relationships between gypsum crystals, and these include:

1. Alabaster texture, which is characterized by fine-grained and oriented nature due to recrystallization and reorientation from their primary rocks as a result

of direct hydration to gypsum [26, 27]. According to textural stages of Holliday (1971) [19], this texture has three stages as follows:

- Stage 1: feathery texture which is common in the lower parts of the Fat'ha Formation as anhedral and sutured crystals of up to 50 micron in size and commonly includes mineral inclusions (**Figure 6A1** and **A2**); it is represented by nodular gypsum lithofacies.
- Stage 2: grained texture, up to 200 micron in size, more clear crystals than the feathery texture with rare inclusions and curved crystal contacts (**Figure 6B1** and **B2**), represented by wispy gypsum lithofacies.
- Stage 3: a developed texture from either stage 1 or stage 2, up to 400 micron in size, subhedral to euhedral crystals with no inclusions, and clear crystal contacts (**Figure 6C1** and **C2**) represented by massive (structureless), compound mosaic and laminated lithofacies.

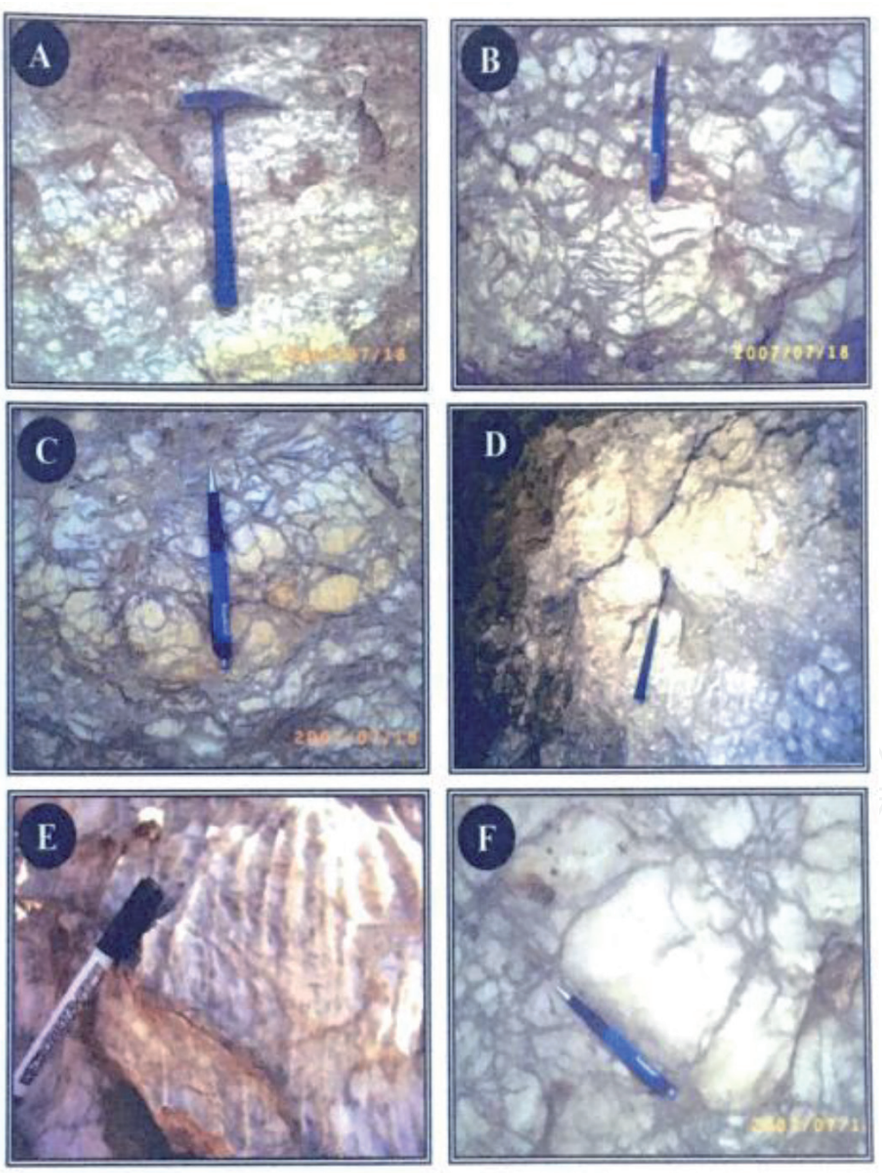

Figure 4.
(A) Mosaic compound gypsum lithofacies, Telkif section; (B) wispy compound gypsum lithofacies, Telkif section; (C) mosaic gypsum lithofacies, Telkif section; (D) graded size in gypsum nodules bed, Sheikh Ibrahim section; (E) wispy gypsum lithofacies, note erosional starching, Sheikh Ibrahim section; (F) massive gypsum lithofacies surrounded by wispy and mosaic lithofacies, Telkif section.

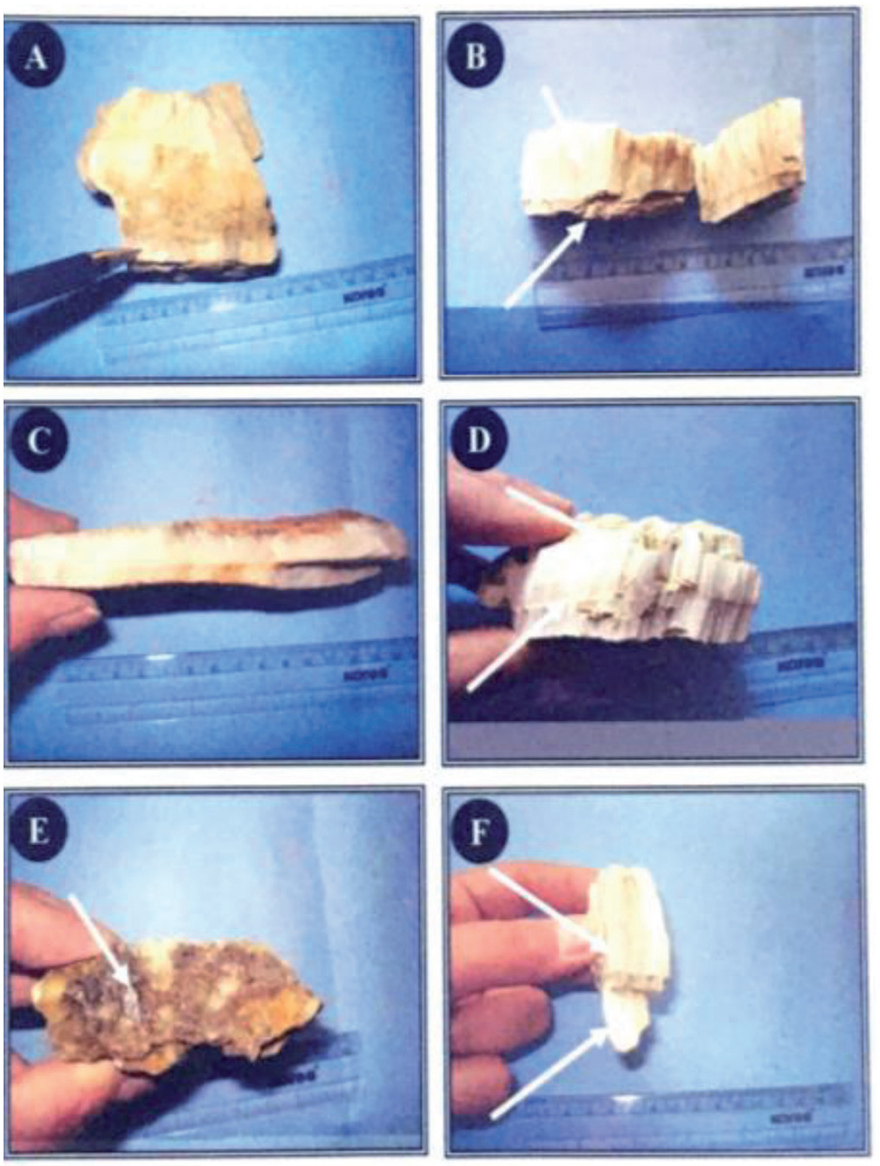

Figure 5.
(A) Gypsum nodule surrounded by fibrous gypsum, Sheikh Ibrahim section; (B) two cross sections of satin spar showing thicker upper lobes, Sheikh Ibrahim section; (C) satin spar veins showing parting in the medium part, Sheikh Ibrahim section; (D) brown mud inclusions in veins of fibrous gypsum, Batnaya section; (E) laminar selenite crystals below satin spar veins, Sheikh Ibrahim section; (F) thick vein of satin spar with curved fibers, Sheikh Ibrahim section.

2. Porphyroblastic texture, which is recognized as large platy crystals with more than 1 cm length which may reflect slow growth of crystals and nuclei [19]. Most of these crystals are embedded in fine alabaster groundmass as a result of anhydrite dissolution and re-precipitation as secondary gypsum (**Figure 7A1** and **A2**). Porphyroblastic texture accompanied also with alabastrine gypsum representing the first growth stage of anhydrite to gypsum (**Figure 7B**). In the field it is represented by mosaic nodular or laminated gypsum lithofacies.

3. Satin spar texture, which commonly are parallel longitudinal fibrous crystals, twinned and oriented with different colors, white, gray and yellow, up to 50 mm long. It is found in either fine (0.11 mm long) (**Figure 8A1** and **A2**) or coarse (0.37 mm) crystals long (**Figure 7C1** and **C2**) represented by fibrous and satin spar lithofacies.

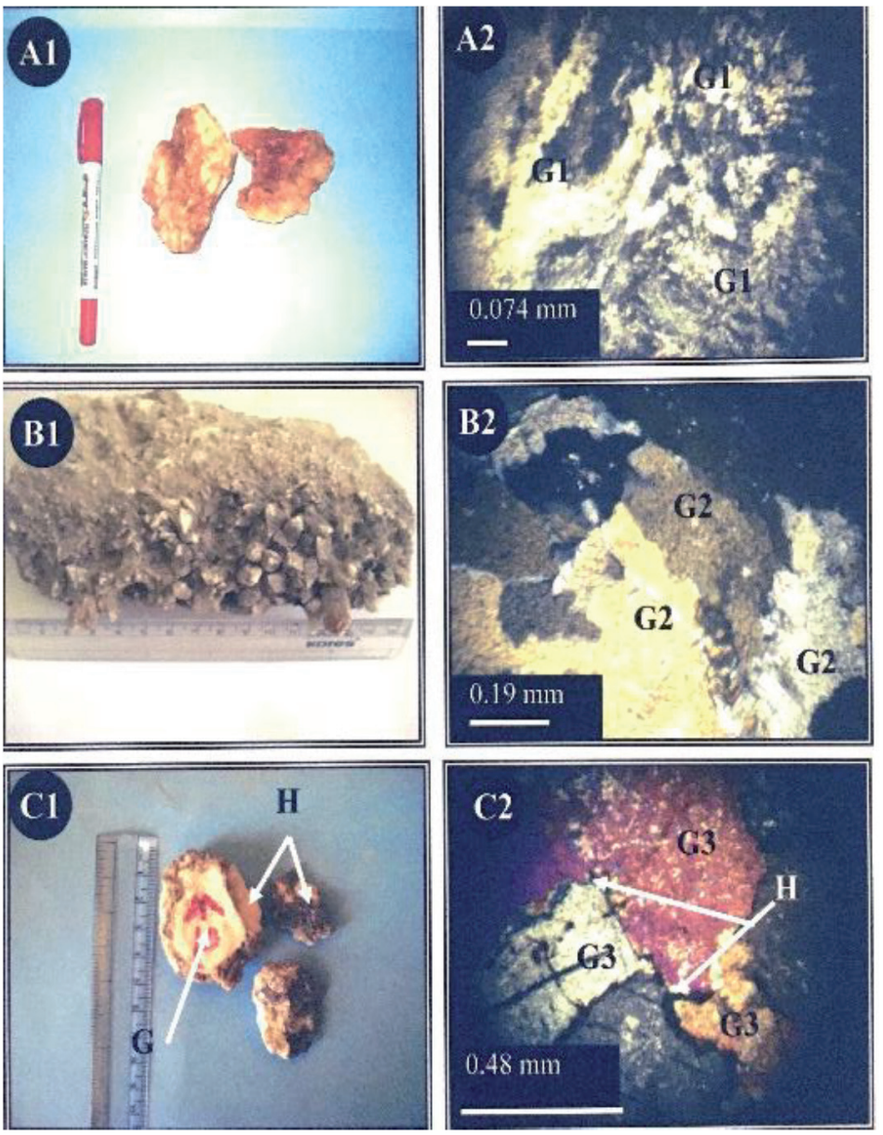

Figure 6.
(A1) Gypsum nodule with brown inclusions, Telkif section; (A2) thin section of the same sample in A1, showing G1 stage of growth of alabastrine gypsum; (B1) gypsum nodules finely crystalline, Sheikh Ibrahim section; (B2) thin section for the same sample in B1 showing G2 growth of alabastrine gypsum; (C1) single gypsum grain (G) surrounded by host carbonate rich in hydrocarbon materials (H), Sheikh Ibrahim section; and (C2) thin section of the same sample in C1 showing G3 growth of alabastrine gypsum and hosting carbonates.

4. Granular texture, which is medium to coarse grained. It exists in two forms as follows:

   - Integrated granular: interconnected crystals of 0.1–0.55 mm in size, represented by nodular gypsum lithofacies (**Figure 8B1** and **B2**).
   - Unintegrated granular: 0.11–0.29 mm size grains of angular edges and also represented by the nodular gypsum lithofacies (**Figure 8C1** and **C2**).

Anhydrite textures: These textures are distinguished in the subsurface sections of the Fat'ha Formation. Based on the crystal shape and size of the anhydrite, six textures are distinguished, these are as follows:

1. Felty texture: crystals in the form of plates of 0.5 mm long with random distribution of crystals which form the advanced stage of recrystallization of finely

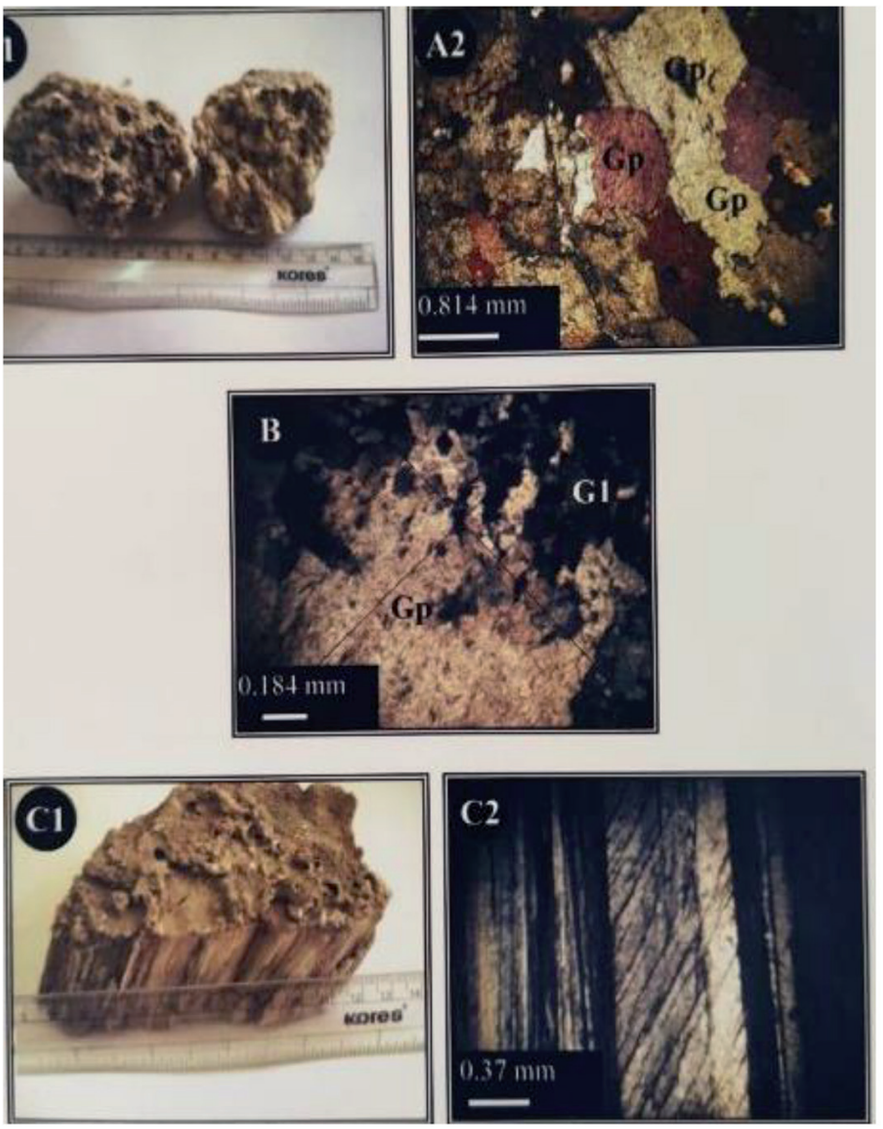

Figure 7.
(A1) Fine mosaic gypsum nodule, Sheikh Ibrahim section; (A2) thin section of the same sample A1 showing porphyroblastic gypsum crystals; (B) thin section of mosaic gypsum showing porphyroblastic texture (Gp) accompanied with alabastrine texture that represent G1 stage of gypsum growth, Telkif section; (C1) satin spar with coarse acicular crystals, Sheikh Ibrahim section; (C2) thin section of the same sample C1 showing coarse fibrous gypsum fibers.

crystalized textures. Hydrocarbon materials are concentrated between crystals (**Figure 9A1** and **A2**).

2. Lath texture: long euhedral plates. They are arranged subparallel to radial forms. Commonly they are distributed in groundmass of felty texture anhydrite (**Figure 9B1** and **B2**).

3. Gneissoid texture: oriented parallel plates presented in curved (v) shape "Chevron" folded shape, which may be formed due to gypsum to anhydrite under high-pressure conditions [28] (**Figure 10A1** and **A2**).

4. Microcrystalline texture: fine crystalline below 0.06 mm in size and equidimensional, accompanied with sub-felty textures (**Figure 10B1** and **B2**).

5. Bacillar texture: fine bladed to prismatic in shape with hydrocarbon materials within this texture (**Figure 11A1–A3**)

6. Porphyroblastic texture: medium-sized (0.2–0.3 mm) anhedral crystals that may reflect advanced stage in anhydrite growth (**Figure 10C1** and **C2**), hydrocarbon also present, (**Figure 11B1** and **B2**).

4.2.2 Diagenetic processes

Due to high solubility of evaporates and their rapid susceptibility to deformation and destruction, most evaporitic succession commonly are changed or deformed after deposition and burial; therefore, it is seldom to find evaporates of primary origin in the geologic record of age earlier than 25my [29].

Facies analysis and petrographic description of the studied evaporates revealed that several diagenetic processes have affected on the studied rocks; these include dehydration (e.g., presence of fine pseudo-gypsum plates with anhydrite), cementation (e.g., either presence of calcareous gypsum plates filling cavities or calcite cementing materials around gypsum nodules), compaction (e.g., continuous growth and suturing of gypsum nodules), hydration (or gypsification, e.g., various

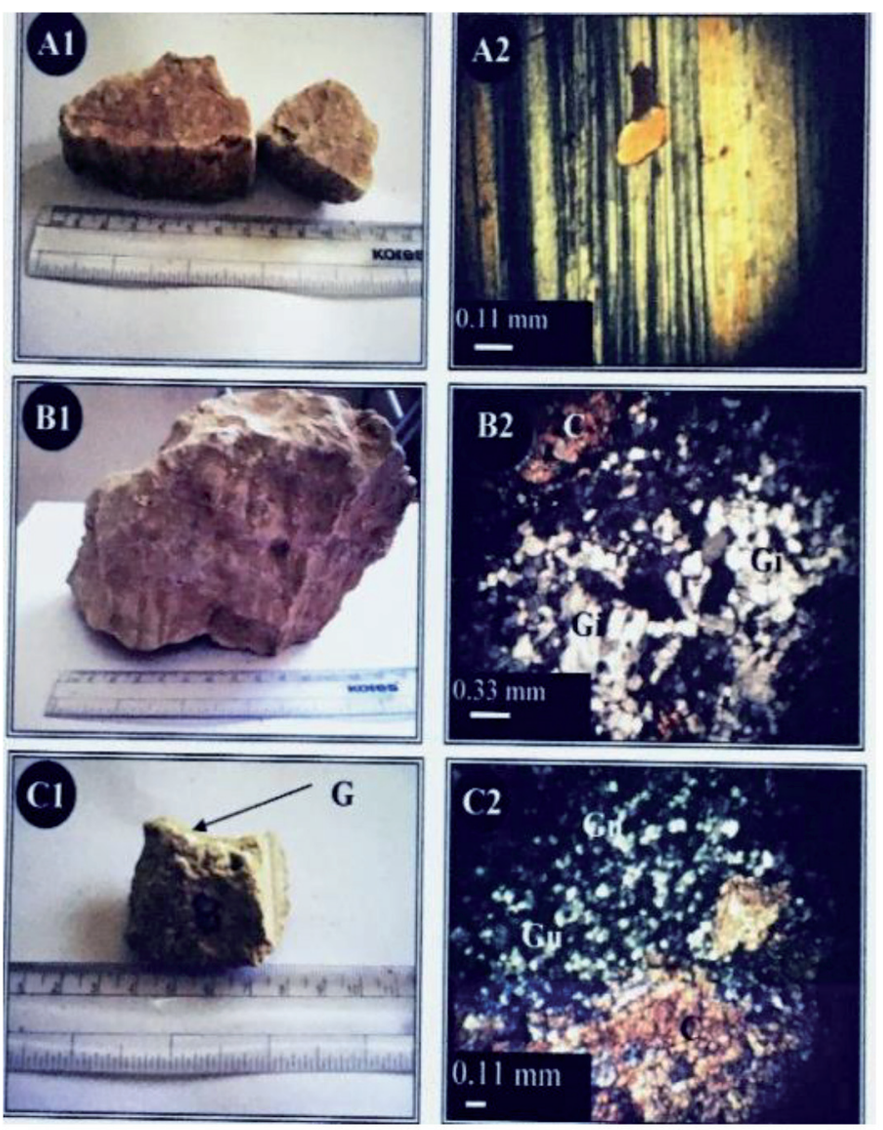

Figure 8.
(A1) Fine secondary satin spar gypsum with fine acicular crystals, Batnaya section; (A2) thin section of the same sample in A1, showing twinning in fine fibrous gypsum; (B1) compound mosaic gypsum nodule, Telkif section; (B2) thin section for the same sample in B1 showing growth in granular gypsum (Gi) with calcite crystals (C) colored red by alizarin red stain; (C1) carbonate grain including very fine gypsum nodule (G), Telkif section; (C2) thin section of the same sample C1 showing granular gypsum with no growth (Gu) surrounded by calcite stained red crystal (C).

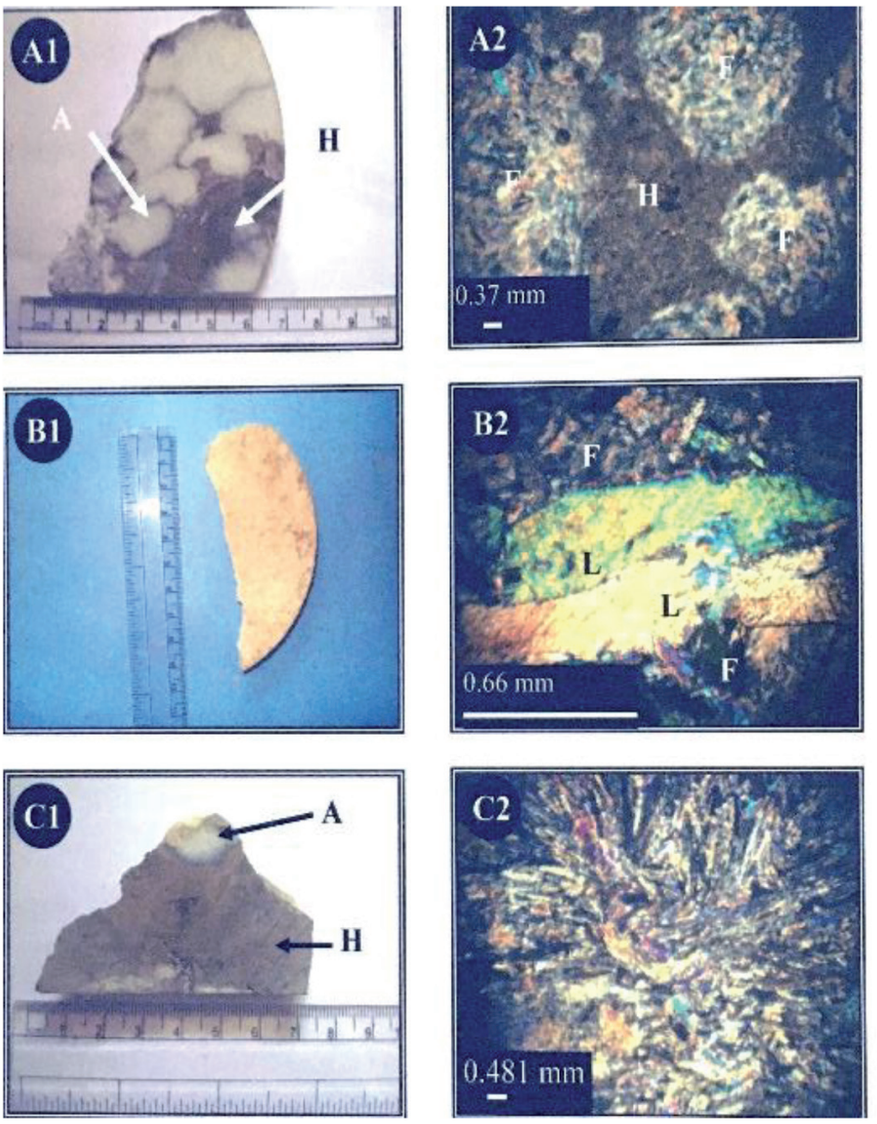

Figure 9.
(A1) Nodular anhydrite (A) with interstitial carbonates rich in hydrocarbons (H), Kirkuk well; (A2) thin section of the same sample in A1, showing felty texture (F), note hydrocarbon existing only on the interstitial materials; (B1) part of pure anhydrite nodule, Kirkuk well; (B2) thin section for the same sample in B1 showing the platy anhydrite in the felty texture; (C1) carbonate including fine anhydrite nodules (A) showing hydrocarbon (H) disseminated in host ground mass not in the anhydrite nodules, Kirkuk well; (C2) thin section of the same sample in C1 showing Chevron folding in anhydrite nodule.

secondary textures such as alabastrine, porphyroblastic, and common satin spar veins), replacement (e.g., calcite replacing gypsum and vice versa), and recrystallization (commonly in the subsurface anhydritic samples, e.g., presence of chevron folding and flow structures). These characteristic features of diagenesis are shown in the previous section and the **Figures 2–11**.

Scanning electron microscopic investigation shows deep focusing various gypsum structures such as coarse crystalline associated with calcite bands (**Figure 12A**) and alternated bands of dark and white folias in the selentic (fibrous) gypsum (**Figure 12B–D**) with carbonate inclusions.

XRD analysis revealed that gypsum is the common mineralogical phase in all the studied samples (**Figure 13**) in addition to rare calcite and/dolomite.

4.3 Geochemistry

Major and trace elements geochemical data for selected gypsum samples are illustrated in **Table 1**. In general, the low content of silica and alumina reflects the

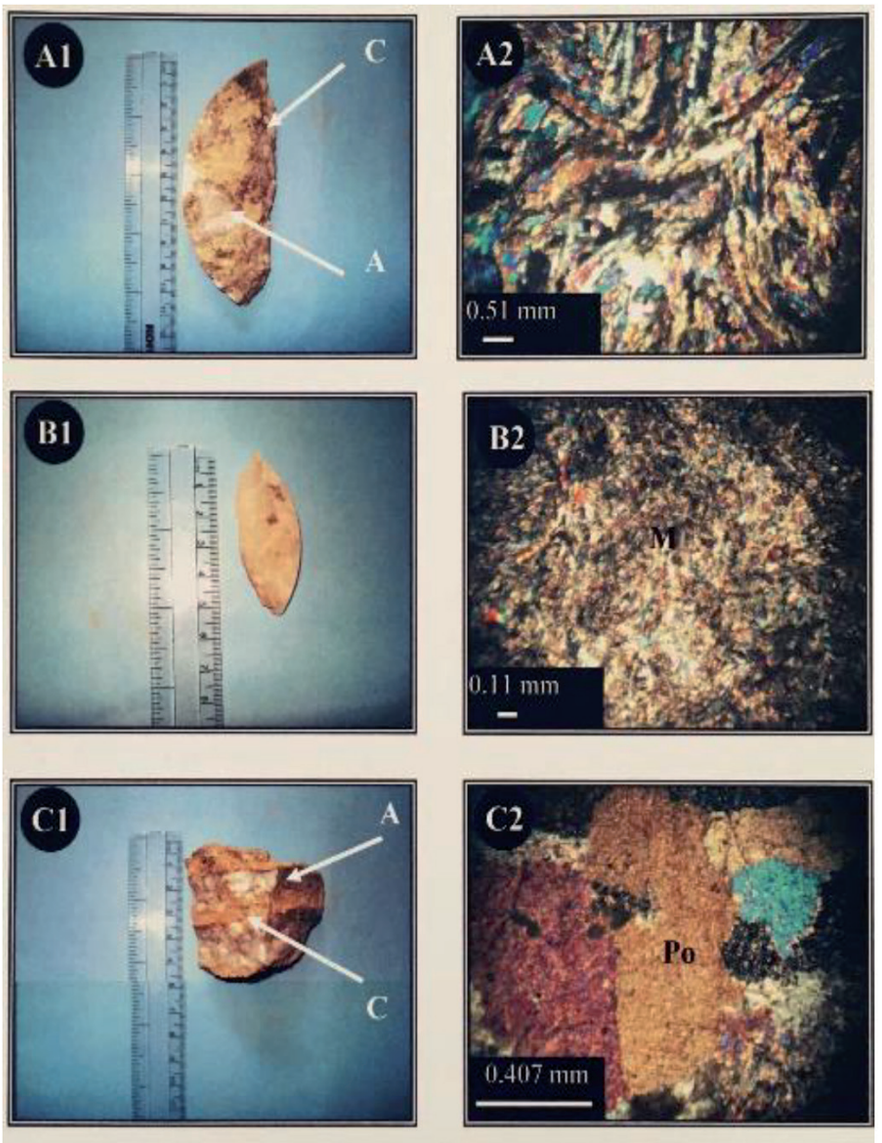

Figure 10.
(A1) Fine anhydrite nodule (A) in carbonate specimen (C), Kirkuk well; (A2) thin section of the same sample in A1, showing flow structures in anhydrite; (B1) finely crystalline anhydrite nodule, Kirkuk well; (B2) thin section for the same sample in B1 showing microcrystalline texture; (C1) finely intercalations of anhydrite nodules (A) and carbonates (C), Kirkuk well; (C2) thin section of the same sample C1 showing porphyroblastic texture (Po).

presence of fine clayey materials in the studied evaporates as brown and gray inclusions. Calcium and magnesium content reflects the accompanied carbonate grains as seen by the petrographic and mineralogic (XRD) investigations in the form of calcite and/or dolomite in addition to calcium in the structure of both gypsum and anhydrites as well as sulfate which is represented by high values of SO_3 (**Table 1**). Trace element distribution of barium and strontium shows high values in mosaic, nodular, and nodular gypsum as compared to laminated and secondary selenite gypsum.

4.4 Efficiency as seal rocks

Porosity and permeability for selected intercalated evaporates and limestone samples from the Fat'ha Formation show that nodular gypsum lithofacies has higher capacity to lock hydrocarbons than the limestone due to very low porosity and permeability (see **Table 2**).

Size of gypsum/anhydrite nodules is an index to the porosity of their groundmass or matrix [30]. In the current work, it seems that chicken wire and

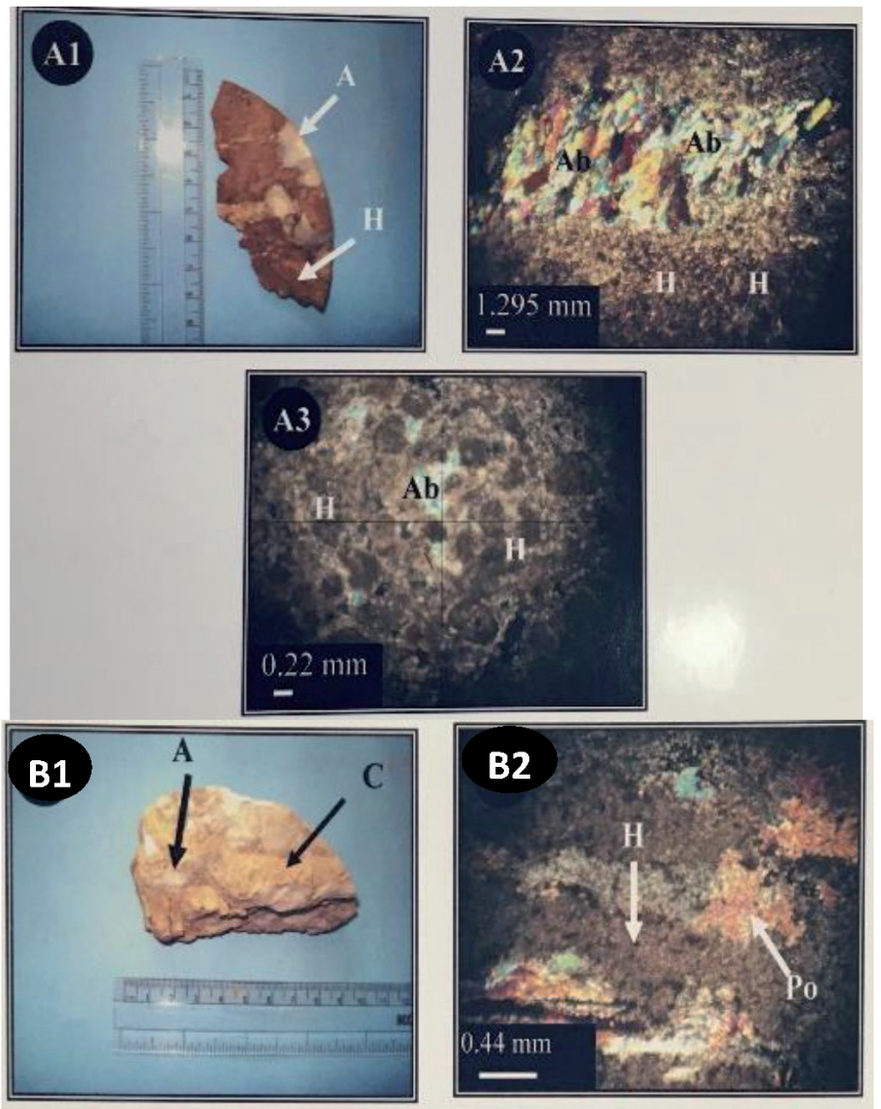

Figure 11.
(A1) Carbonate grain highly enriched in hydrocarbons (H) in which anhedral pure anhydrite nodules (A) are present, Kirkuk well; (A2–A3) thin section of the same sample in A1, showing basilar texture (Ab) and hydrocarbons (H); (B1) carbonate grain (C) with fine anhydrite, Kirkuk well; (B2) porphyroblastic texture of anhydrite embedded in hydrocarbon-rich materials.

enterolithic structures are common in the granular porous matrix; these structures required porous materials with solution movements to form [30]. The Fat'ha Formation evaporites are commonly of large-sized nodules embedded in granular matrix. This matrix could be principally porous that allow some hydrocarbons to disseminate. Consequently, when nodules grow and are compacted as a result of dehydration and compaction, the matrix porosity decreased, and the hydrocarbons were locked.

Petrographic study revealed that bituminous materials are locked in between anhydrite nodules within basilar (**Figure 11A1** and **A2**) and porphyoblastic (**Figure 11B1** and **B2**) textures that may refer to the important role of these anhydritic nodules in locking hydrocarbons.

However, gypsum nodules that formed by hydration of anhydrite, bituminous materials were found in the contact between alabastrine gypsum nodules (**Figure 6C1** and **C2**) that are represented by massive and wispy lithofacies, which may play a role in locking hydrocarbons.

Field study revealed that thick limestones (units A and C) enriched with bitumen in the lower member of the Fat'ha Formation are common below the mosaic

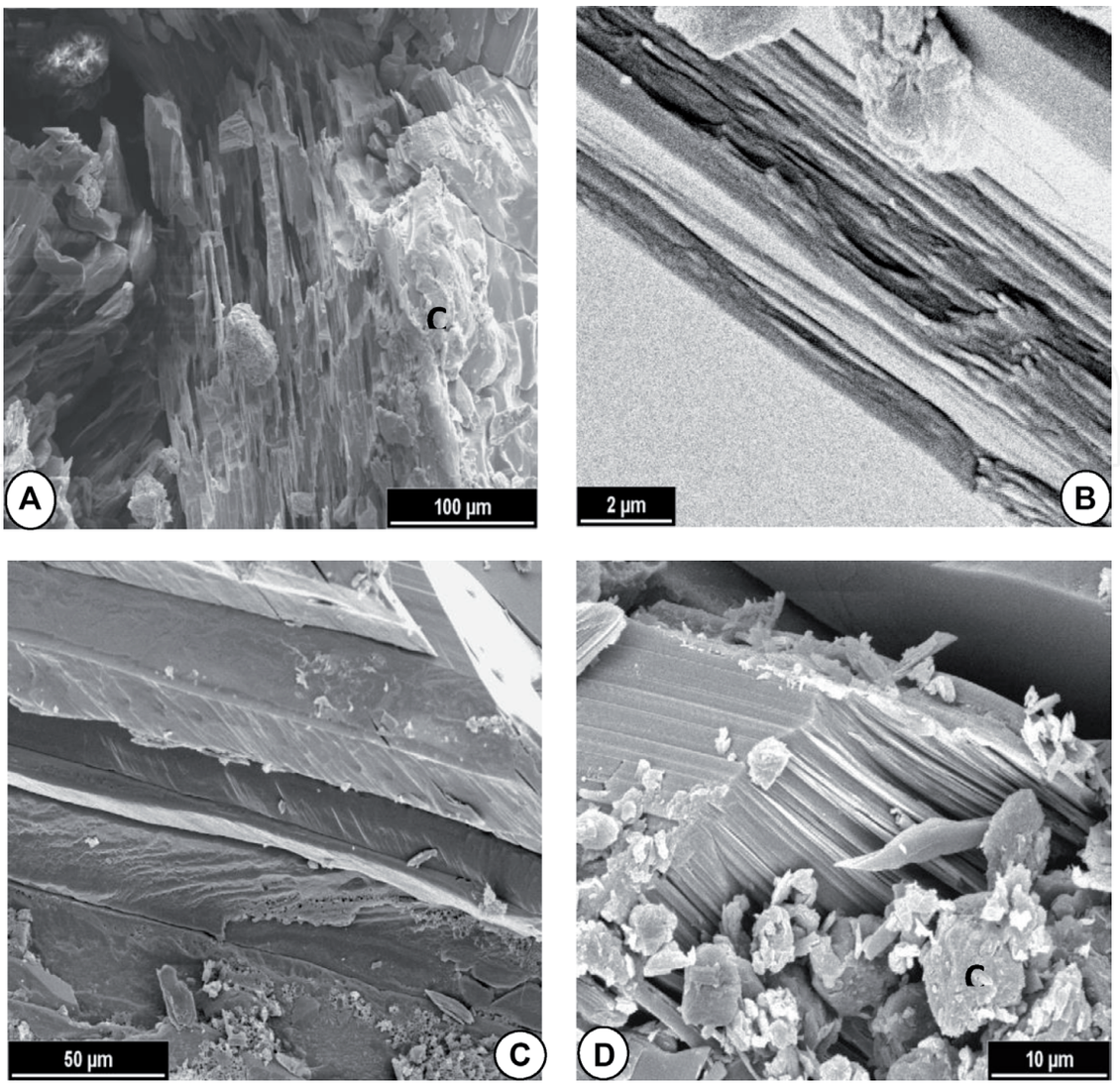

Figure 12.
SEM images show (A) coarse crystalline gypsum with scattered fine calcite (C) in a band that may be responsible for the gray color of the gypsum. (B) Alternating white and dark folia in selenitic gypsum. (C) Foliated nature of selenitic gypsum. (D) Broken folias of selenite with carbonate inclusions (C), Sheikh Ibrahim section.

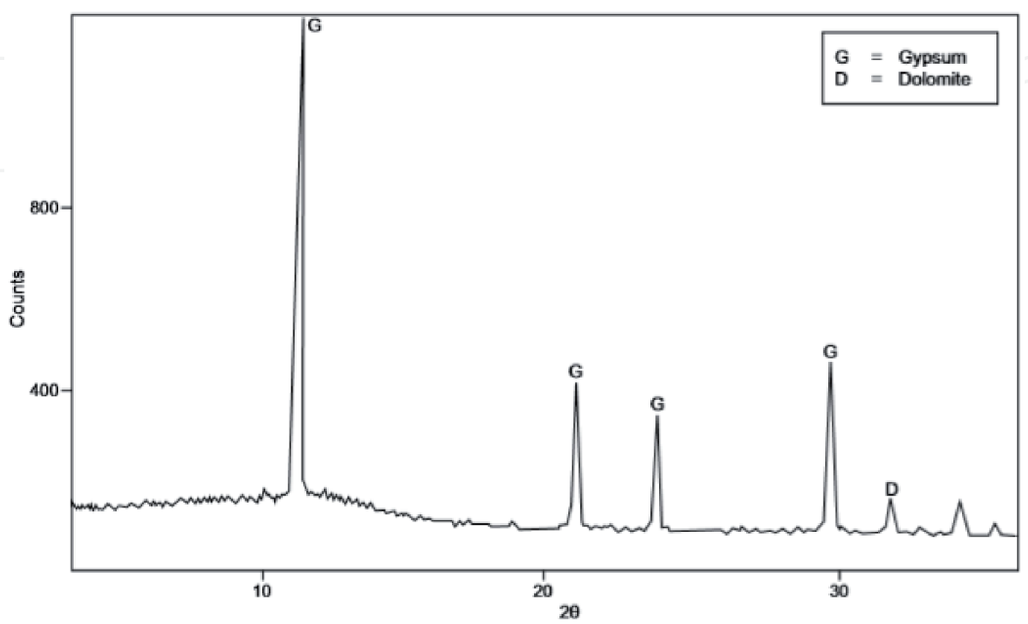

Figure 13.
XRD scan of nodular gypsum sample from the Fat'ha Formation in sheikh Ibrahim section illustrating the common presence of gypsum with rare dolomite.

Gypsum type	SiO_2 (%)	Al_2O (%)	TiO_2 (%)	MnO (%)	MgO (%)	CaO (%)	K_2O (%)	Na_2O (%)	Fe_2O_3 (%)	P_2O_5 (%)	SO_3 (%)	Ba ppm	Sr ppm
Nodular	1.4	0.4	0.02	0.01	0.2	18	0.01	0.1	0.02	0.03	48	2.8	246
Laminated	3.0	0.9	0.03	0.01	1.9	19.5	0.08	0.1	0.1	0.03	46	1.4	110
Massive	1.6	0.5	0.02	0.01	0.4	18.2	0.01	0.14	0.02	0.03	48	0.6	245
Gypsum-anhydrite mosaic	1.8	1.4	0.01	0.01	0.3	18.4	0.01	0.08	0.03	0.03	47	4.6	615
Brown massive	2.2	0.7	0.03	0.01	0.7	18.2	0.02	0.2	0.04	0.03	48	4.5	201
Wispy	2.9	0.9	0.03	0.01	1.8	19	0.07	0.1	0.11	0.03	46	1.2	113
Selenite	2.4	0.7	0.03	0.01	0.7	18.6	0.03	0.2	0.05	0.03	48	1.8	83

Table 1.
Geochemical data of selected gypsum samples of the Fat'ha Formation in Sheikh Ibrahim section.

Sample	Description	Porosity (%)
K1	Pure anhydrite	0.25
K2	Anhydrite with impurities	4.0
K3	Limestone	17
T1	Surface gypsum sample	0.9

Table 2.
Porosity data for selected samples.

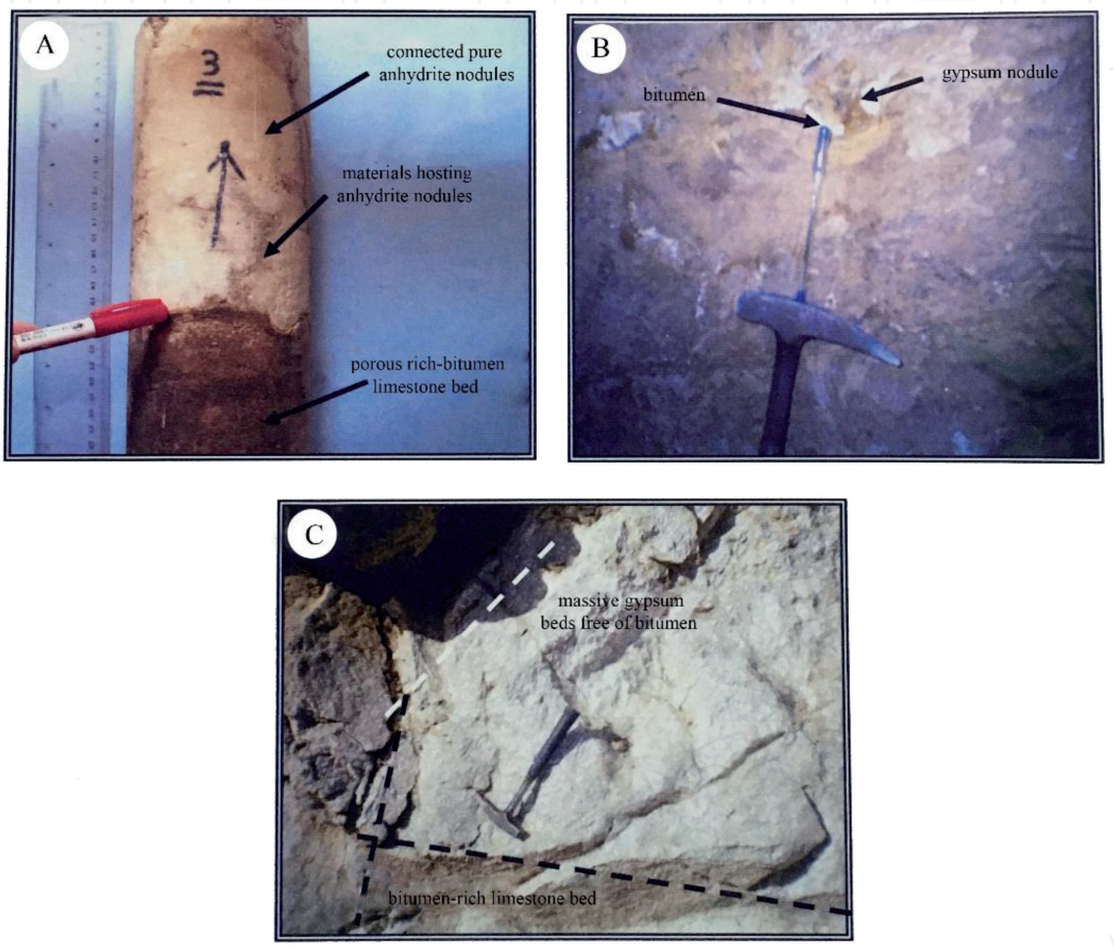

Figure 14.
Core and field images showing (A) core from Kirkuk well illustrates the nature of contact between the porous bitumen-rich limestone in the lower part and compact pore-free anhydrite bed; note some early disseminated hydrocarbons in the host materials (arrows). (B) Bed of nodular gypsum hosting brown hydrocarbon-rich matrix, Sheikh Ibrahim section. (C) Bitumen-rich limestone overlaid by hydrocarbon-free gypsum bed, Sheikh Ibrahim section.

gypsum beds. This gypsum beds may represent seal or cap rocks of the Fat'ha Formation (**Figure 14**). Permeability data show that it is low in the studied gypsum rocks.

5. Discussion and conclusions

Evaporites are indicative for arid continental environments [29], and their formation in sedimentary basins depends mostly on the connection of this basin with oceanic or sea water. Where this connection is periodically interrupted within

arid settings, this may led to high evaporation of the basin and cyclic deposition of evaporitic successions in the sedimentary basins [31].

Lithofacies analysis of the studied evaporates revealed the presence of nodular and massive gypsum/anhydrite, laminated gypsum and secondary selenite, and satin spar lithofacies with several sublithofacies; these are representative of relict basin evaporate deposition based on their tectonic setting which they deposited during closure periods of the Neo-Tethys basin on the northern Arabian Plate passive margins [32].

Due to wide distribution of the Fat'ha Formation, several ideas have been proposed for the depositional cycles of gypsum formation. Semi-restricted lagoonal environments such as lakes which were connected to the open sea through narrow channels coincide with the brine-filled basin model suggested by [33, 34], while sabkha or supratidal flat depositional setting and coastal or inland sabkhas with semiarid shallow lagoon were favored by [18, 32], respectively. These models could be comparable with the Messinian basin evaporites of the Mediterranean [35] and Middle Miocene (Badenian) basin-marginal evaporites of the Carpathian Foredeep basin of western Ukraine [36].

Petrographic investigation of the gypsum and anhydritic rocks of the Middle Miocene Fat'ha Formation has revealed that nodular gypsum is the dominant type and is composed of granular integrated gypsum texture with evidence of recrystallization, whereas alabastrine texture is the common type in the laminated gypsum. Secondary gypsum of selenite and satin spar shows alabastrine, fine to coarse fibrous, and porphyroblastic textures with the alabastrine type being predominant.

Nodular gypsum was deposited in a very shallow, arid, and semi-restricted lagoonal environment which has undergone influx and reflux processes, while laminated gypsum may represent pulses of freshwater into the lagoonal basin of Fat'ha Formation.

The chemical composition of selected nodular, laminated, and secondary (selenite) and mosaic gypsum shows low values of strontium (Sr) in the secondary and laminated types due to their secondary origin by the hydration from the original anhydrite through which Sr. in the original anhydrite was expelled. The impoverishment in Sr. commonly occurs in secondary-type gypsum as compared with primary ones [37]. High values in some of gypsum types (see **Table 1**) may be attributed to diagenetic processes and the sea salinity.

Hydrocarbons present mainly in the limestone beds underlie gypsum beds and in materials hosting gypsum nodules. Porous granular texture of these materials allowed hydrocarbon inclusion, later on, during compaction and growth of nodular to compound mosaic due to recrystallization resulted in prevent hydrocarbon dissemination, then these materials were locked in these materials and partly in accompanied gypsum nodules. These results were revealed by low porosity and permeability of the studied gypsum nodules as compared to those of the limestone beds.

DOI: http://dx.doi.org/10.5772/intechopen.92566

Author details

Ali I. Al-Juboury[1*], Rana A. Mahmood[2] and Abulaziz M. Al-Hamdani[1]

1 Department of Geology, College of Sciences, University of Mosul, Mosul, Iraq

2 College of Electrical Engineering, Ninevah University, Mosul, Iraq

*Address all correspondence to: alialjubory@yahoo.com

References

[1] Yi-gang Z. Cool shallow origin of petroleum-microbial genesis and subsequent degradation. Journal of Petroleum Geology. 1981;**3**:427-444

[2] Warren JK. Evaporite Sedimentology: Importance in Hydrocarbon Accumulation. Englewood Cliffs: Prentice Hall; 2014. p. 285

[3] Al-Juboury AI, McCann T. The middle Miocene Fat'ha (lower Fars) Formation of Iraq. GeoArabia. 2008;**13**(3):141-174

[4] Dunnington HV. Generation, accumulation and dissipation of oil in northern Iraq. In: Weeks LG, editor. Habitat of Oil. USA: American Association of Petroleum Geologists; 1958. pp. 1194-1251

[5] Buday T. The regional of Iraq. In: Stratigraphy and Palaeogeography. Vol. 1. Baghdad, Iraq: State Organization for Minerals; 1980. p. 445

[6] Goff JC, Jones RW, Horbury AD. Cenozoic basin evolution of the northern part of the Arabian Plate and its control on hydrocarbon habitat. In: Al-Husseini MI, editor. Middle East Petroleum Geosciences Conference, GEO'94. Vol. 1. Bahrain: Gulf PetroLink; 1995. pp. 402-412

[7] Numan NMS. A plate tectonic scenario for the Phanerozoic succession in Iraq. Journal of the Geological Society of Iraq. 1997;**30**:85-110

[8] Al-Juboury AI, Al-Naqib SQ, Al-Juboury AMS. Sedimentology, mineralogy and depositional environments of the clastic units, Fat'ha Formation (middle Miocene), south of Mosul, Iraq. Dirasat, Pure Sciences, Jordan. 2001;**28**:80-105

[9] Van Bellen RC, Dunnington H, Wetzel R, Morton DM. Lexique Stratigraphique International. Paris: Centre National Recherché Scientifique, Fasc 10a, Iraq; 1959. p. 333

[10] Metwalli MH, Philip G, Moussly MM. Petroleum-bearing formations in northeastern Syria and northern Iraq. American Association of Petroleum Geologists Bulletin. 1974;**58**:1781-1796

[11] Beydoun ZR. Arabian plate hydrocarbon geology and potential: A plate tectonic approach. American Association of Petroleum Geologists, Studies in Geology. 1991;**33**:1-77

[12] Sharland PR, Archer R, Casey DM, Davies RB, Hall SH, Heward AP, et al. Arabian Plate Sequence Stratigraphy. Bahrain: GeoArabia Special Publication 2, Gulf PetroLink; 2001. p. 371

[13] Buday T, Jassim SZ. The Regional Geology of Iraq, Tectonism, Magmatism and Metamorphism. Baghdad, Iraq: Publication of the Geological Survey of Iraq; 1987. p. 352

[14] Al-Sharhan AS, Nairn AEM. Sedimentary Basins and Petroleum Geology of the Middle East. Amsterdam: Elsevier; 1997. p. 843

[15] Jordan TE. Thrust loads and foreland basin evolution, cretaceous, western United States. Bulletin of the American Association of Petroleum Geologists. 1981;**65**:2506-2520

[16] Allen PA, Homewood P, Williams GD. Foreland basins: An introduction. In: Allen PA, Homewood P, editors. Foreland Basins. Vol. 8. International Association of Sedimentologists, Special Publication. Berlin, New York: Springer; 1986. pp. 3-12

[17] Al-Sawaf FDS. Sulfate reduction and sulfur deposition in the lower Fars formation, northern Iraq. Economic Geology. 1977;**72**:608-618

[18] Shawkat MG, Tucker ME. 1978. Stromatolites and sabkha cycles from the lower Fars formation (Miocene)

of Iraq. Geologische Rundschau. 1978;**67**:1-14

[19] Holliday DW. Origin of lower Eocene gypsum-anhydrite rocks, south eastern St Andrew, Jamaica. Applied Earth Science. 1971;**80**:305-315

[20] Maiklem WR, Bebout DC, Glaister RP. Classification of anhydrite—A practical approach. Bulletin of Canadian Petroleum Geology. 1969;**17**:194-233

[21] Meyer FO. Anhydrite Classification According to Structure. 2005. Available from: http://www.crienterprises.com/Edu_Classif_Evahtml

[22] Sarg JF. Petrology of the carbonate-evaporite facies transition of the seven Rivers formation (Guadalupian, Permian), Southeast New Mexico. Journal of Sedimentary Petrology. 1981;**51**:73-93

[23] Paz JDS, Rossetti DF. Petrography of gypsum-bearing facies of the Codo formation (late Aptian), northern Brazil. Annals of the Brazilian Academy of Science. 2006;**78**(3):557-572

[24] Orti F, Rosell L. The Ninyerola gypsum unit: An example of cyclic, lacustrine sedimentation (middle Miocene, E Spain). Journal of Iberian Geology. 2007;**33**(2):249-260

[25] Bedelean H. Considerations on the parent material in the soil developed on the evaporate deposits from Stana. Geologica. 2003;**XL**(2):59-66

[26] Murray RC. Origin and diagenesis of gypsum and anhydrite. Journal of Sedimentray Research. 1964;**34**(3):512-523

[27] Warren JK. Evaporites: Sediments, Resources and Hydrocarbons. Berlin, New York: Springer; 2006. p. 1035

[28] Blatt H, Middeleton G, Murray R. Origin of Sedimentary Rocks. New Jersey: Prentice-Hall Inc.; 1972. p. 634

[29] Boggs SJ. Principles of Sedimentology and Stratigraphy. New Jersey: Pearson Prentice-Hall; 2006. p. 662

[30] Shearman DJ, Fuller JG. Anhydrite diagenesis, calcitization and organic laminates, Winnipegosis formation, middle Devonian, Saskatchewan. Bulletin the Canadian Petroleum Geology. 1969;**17**:496-525

[31] Nichols G. Sedimentology and Stratigraphy. Oxford: Blackwell Scientific Publications; 1999. p. 355

[32] Mustafa AAM. Sedimentological studies of the lower fars formation in the Sinjar Basin, Iraq [MSc thesis]. Iraq: Mosul University; 1980; p. 243 [Unpublished]

[33] Sulayman MD. Geochemistry, petrology, origin and diagenesis of gypsum rocks of lower fars formation at Butma West area, northern Iraq [MSc thesis]. Iraq: Mosul University; 1990; p. 175 [Unpublished]

[34] Jassim RZ. Gypsum deposits in Iraq: An overview. Iraqi Bulletin of Geology and Mining. 2019;**8**:241-261

[35] Rouchy JM, Taberner C, Blanc-Valleron MM, Sprovieri R, Russell M, Pierre C, et al. Sedimentary and diagenetic markers of the restriction in a marine basin: The Lorca Basin (SE Spain) during the Messinian. Sedimentary Geology. 1998;**121**:23-55

[36] Peryt TM. Gypsum facies transitions in basin-marginal evaporites: Middle Miocene (Badenian) of West Ukraine. Sedimentology. 2001;**48**:1103-1119

[37] Playa E, Orti F, Rosell FL. Marine to non-marine sedimentation in the upper Miocene evaporites of the eastern Betics, SE Spain: Sedimentological and geochemical evidence. Sedimentary Geology. 2000;133(1-2):135-166